Neutral air turbulence and temperatures in the vicinity of polar mesosphere summer echoes

Franz-Josef Lübken, Markus Rapp, and Peter Hoffmann
Leibniz-Institut für Atmosphärenphysik, Kühlungsborn, Germany

Received 4 June 2001; revised 29 November 2001; accepted 30 November 2001; published 15 August 2002.

[1] A total of 8 sounding rocket flights with measurements of neutral air turbulence in the upper mesosphere have been performed in the past 10 years with simultaneous and nearly co-located radar measurements of polar mesosphere summer echoes (PMSE). These measurements took place close to the rocket ranges in northern Norway (Andøya Rocket Range, 69°N) and in northern Sweden (Esrange, 68°N). A detailed comparison demonstrates that there is no apparent correlation between PMSE and neutral air turbulence and that in fact turbulence is absent in the majority of all PMSE events (no turbulence in 7 out of 10 PMSE layers). This suggests that neutral turbulence and other mechanisms affecting the neutral atmosphere at very small spatial scales play a minor role in creating PMSE, contrary to the speculations published in the literature. The main mechanism for creating PMSE remains unidentified. A comparison of PMSE with simultaneous temperature profiles derived from falling sphere and ionization gauge measurements shows that PMSE are practically always present at altitudes where the temperature is low enough for water ice particles to exist. This supports the general understanding that PMSE are closely related to charged water ice particles. On the other hand, the measurements also demonstrate that low enough temperatures are not sufficient for PMSE to exist. Temperature lapse rates were deduced from the high-altitude-resolution ionization gauge measurements. Within the PMSE layers the temperature lapse rate is typically +1–2 K/km with a rather large variability of ±5–10 K/km. Adiabatic lapse rates have never been found within a PMSE layer, which suggests that turbulence cannot have been active for a substantial period. This again supports the idea that neutral air turbulence plays a minor role in creating PMSE. Probably the only common physical reason for PMSE and turbulence is the background temperature profile, which supports the creation of ice particles (since temperatures are very low) and which provokes the breaking of gravity waves and creation of turbulence since the temperature gradient changes at the mesopause. *INDEX TERMS:* 0350 Atmospheric Composition and Structure: Pressure, density, and temperature; 3332 Meteorology and Atmospheric Dynamics: Mesospheric dynamics; 3379 Meteorology and Atmospheric Dynamics: Turbulence; 2439 Ionosphere: Ionospheric irregularities; 6952 Radio Science: Radar atmospheric physics; *KEYWORDS:* summer mesosphere, PMSE, turbulence (neutral and plasma), cold mesopause, temperatures (thermal structure) in the upper atmosphere, radars and sounding rockets

1. Introduction

[2] Very strong radar echoes called "polar mesosphere summer echoes" (PMSE) were first observed at frequencies around 50 MHz (VHF band) more than 20 years ago [*Czechowsky et al.*, 1979; *Ecklund and Balsley*, 1981]. Later observations by various radars operating at different frequencies confirmed that these very intense echoes occur only during summer and mainly from a few kilometers below the mesopause (see review by *Cho and Röttger* [1997]). The explanations given for PMSE were mostly related to neutral air turbulence which was believed to cause small-scale fluctuations also in the plasma density and thereby creates refractive index variations at the Bragg scale of the radar waves (=$\lambda/2\sim$3 m for a 50 MHz radar). It was quickly realized that unrealistically large neutral turbulence intensities are required to create significant fluctuations at such small spatial scales since turbulence is effectively damped by viscous dissipation. In the classical theory of turbulence the transition between the spectral subrange affected by viscous dissipation ("viscous subrange") and those spatial scales where inertial forces determine the cascading from large to small scales ("inertial subrange") is given by the inner scale $l_\circ^H = 9.90 \cdot \eta = 9.90 \cdot (\nu^3/\epsilon)^{1/4}$ where $\eta = (\nu^3/\epsilon)^{1/4}$ is the so called "Kolmogoroff microscale," ν is the kinematic viscosity, and ϵ is the turbulent energy dissipation rate [*Tatarskii*, 1971; *Lübken*, 1997] (the superscript H in $l_\circ^H$ indicates that the theoretical spectrum goes back to Heisenberg). Roughly speaking the Bragg scale $\lambda/2$ has to be larger than $l_\circ^H$ to allow for significant fluctuations caused by neutral air turbulence. Since ν is on

0148-0227/02/2001JD000915$09.00

Table 1. Rocket Flights With Ionization Gauge Measurement of Turbulence in the Vicinity of PMSE[a]

Flight Label	Date	Time, UT	Radar
NAT13	Aug. 9, 1991	23:15:00	CUPRI
NBT05	Aug. 1, 1991	01:40:00	CUPRI
SCT03	July 28, 1993	22:23:00	EISCAT
SCT06	July 31, 1993	01:46:00	EISCAT
ECT02	July 28, 1994	22:39:00	ALOMAR/SOUSY
ECT07	July 31, 1994	00:50:33	ALOMAR/SOUSY
ECT12	Aug. 12, 1994	00:53:00	ALOMAR/SOUSY
MDMI05	July 6, 1999	00:06:00	ALWIN

[a] Flight NAT13 and NBT05 took place from Esrange, 68°N (Sweden), and the TOTAL sensor was used in these flights. All other flights took place from Andøya, 69°N (Norway), where the CONE sensor was used. More details on the radars are given in the text.

the order of 1 m^2/s at the summer mesopause extremely strong turbulence of $\epsilon \sim 100$ W/kg is required to fulfill this condition. Such a turbulence intensity corresponds to an unrealistically large heating rate of 86400 K/d (!).

[3] Fluctuations in the plasma leading to PMSE are created by moderate neutral turbulence, however, if the diffusion coefficient D of the plasma is smaller than the kinematic viscosity ν, i.e., that the so called "Schmidt number" $Sc = \nu/D$ is significantly larger than unity. It was proposed by *Kelley et al.* [1987] and by *Cho et al.* [1992] that large cluster ions and charged aerosols, respectively, reduce the mobility of the electrons (since they are electrically bound to the "heavy" aerosols) which allows for fluctuations in the electron gas at very small spatial scales where neutral density fluctuations are destroyed by viscous dissipation. Large Schmidt numbers are expected in these cases. Indeed, simultaneous measurements of small-scale fluctuations of neutral number densities (indicative of neutral air turbulence), electron number densities, and charged aerosols showed a spectral separation at scales close to $l_\odot^H$ at altitudes where charged aerosols are present and gave large Schmidt numbers of up to 385 [*Lübken et al.*, 1994, 1998; *Havnes et al.*, 1996]. The explanation involving charged aerosols is consistent with the presence of water ice particles which can only exist in the summer mesopause region where very low temperatures prevail [*Lübken*, 1999; *Hervig et al.*, 2001]. If large enough, these aerosol particles can be seen from the ground by naked eye or by lidars as so called "noctilucent clouds" [*Gadsden and Schröder*, 1989; *Nussbaumer et al.*, 1996; *von Zahn and Bremer*, 1999].

[4] Common in situ and radar measurements revealed also that PMSE exist at altitudes where no neutral air turbulence is present in which case the theory outlined above fails to explain the small-scale plasma fluctuations required for PMSE [*Lübken et al.*, 1993]. It is the purpose of this paper to summarize the experimental results regarding PMSE, neutral air turbulence, and temperatures.

[5] In the past 10 years a total of 8 sounding rocket flights with small-scale neutral air measurements have been performed simultaneously and nearly co-located with radar detected PMSE. In this paper we review and summarize the results of these measurements. We will concentrate on PMSE in the VHF band since the common in situ and ground based measurements were primarily performed with radars of this type. In section 2 the experimental techniques and the data available are introduced and in section 3 a detailed comparison between ground based radar observations of PMSE and in situ measurements of turbulence and temperatures is presented. The implications and the conclusions from the experimental results are discussed in sections 4 and 5.

2. Measurements

2.1. Neutral Air Turbulence

[6] Since the early 1990s rocket borne in situ measurements of small-scale neutral density fluctuations have been performed and analyzed in terms of turbulence. The main idea behind these measurements is that turbulent velocity fluctuations cause vertical adiabatic excursions of air parcels so that the number density inside these air parcels deviates from the background profile. Turbulence can therefore be detected as small-scale fluctuations in neutral number density relative to a smooth background [*Thrane and Grandal*, 1981; *Lübken*, 1992].

[7] Two versions of an ionization gauge, namely TOTAL (since total number density is measured) and CONE (combined neutral and electron sensor) were developed and launched on sounding rockets during various campaigns from the Andøya Rocket Range (69°N) in northern Norway and from Esrange (68°N) in northern Sweden. Technical details of the instruments are published elsewhere [*Hillert et al.*, 1994; *Giebeler et al.*, 1993]. A list of all flights with ionization gauge measurements of small-scale neutral air densities in the vicinity of PMSE is given in Table 1.

[8] In Figure 1 we show a spectral analysis of relative density fluctuations measured during flight MDMI05 in an altitude bin of 87 ± 1.5 km. The theoretical turbulence spectrum of Heisenberg is fitted to the measurements and the turbulent energy dissipation rate ϵ is obtained from the best fit (see *Lübken* [1992, 1997] for more details). From the

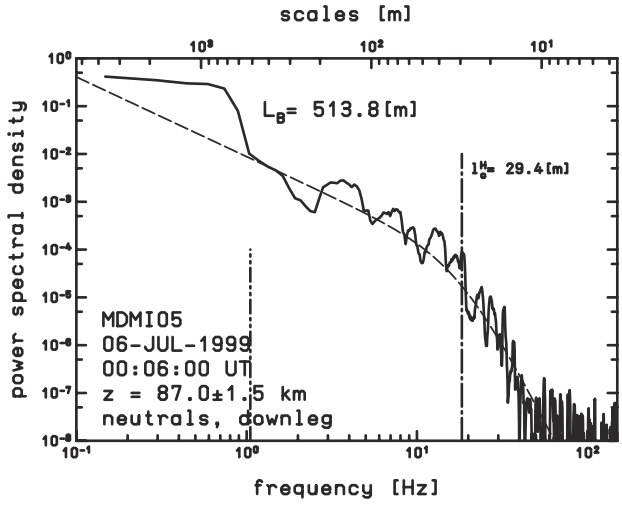

Figure 1. Spectrum of relative density fluctuations in the altitude range 87 ± 1.5 km measured during flight MDMI05. Frequencies f are converted to scales using $\ell = v_R/f$ where $v_R = 539$ km/s is the rocket velocity. The best fit Heisenberg model with an inner scale of $l_\odot^H$=29.4 m is shown as a dashed line. L_B is the so called "outer scale" of turbulence defined as $L_B = 9.97 \cdot \sqrt{\epsilon/\omega_B^3}$.

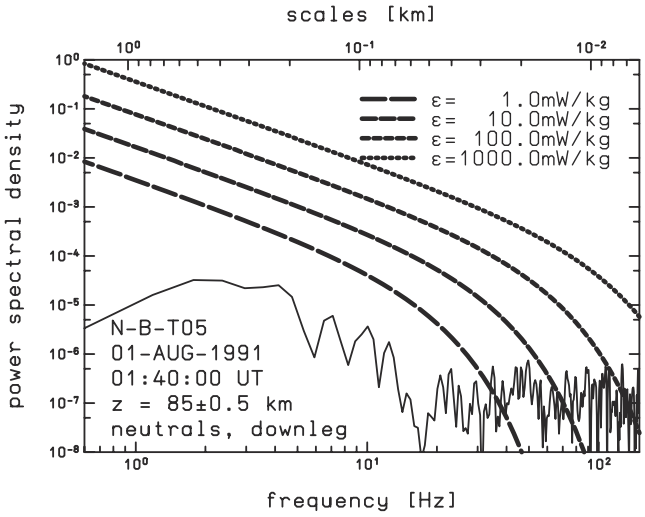

Figure 2. Same as Figure 1 but for fluctuations measured in the altitude range 85 ± 0.5 km during flight NBT05. Several theoretical spectra for various ϵ values are shown for comparison. At the same time the quantity N_θ has been varied by a factor of 10 from $N_\theta = 1 \times 10^{-8}$/s (for $\epsilon = 1$ mW/kg) up to $N_\theta = 1 \times 10^{-5}$/s (for $\epsilon = 1000$ mW/kg). See *Lübken* [1992] for more details. The measured power spectral densities are too small for turbulence even if it were very weak.

spectrum shown in Figure 1 we derive $\epsilon = 77$ mW/kg which corresponds to a heating rate of 6.6 K/d. The inner scale in this example is $l_\circ^H = 29.4$ m, much too large to allow for any significant fluctuations at the radar Bragg scale of 3 m.

[9] In Figure 2 we show a second example of a spectrum measured during flight NBT05 in an altitude bin of 85 ± 0.5 km. The data reduction procedure, i.e., the determination of relative fluctuations, spectral analysis, smoothing etc., is identical to that used in Figure 1. For comparison we show four theoretical spectra for very small up to strong turbulence (ϵ is varied by a factor of 10 from 1 to 1000 mW/kg). At the same time we have varied the quantity N_θ (which appears in the theoretical description of the turbulent spectrum) by a factor of 10 from $N_\theta = 1 \times 10^{-8}$/s for the $\epsilon = 1$ mW/kg profile up to $N_\theta = 1 \times 10^{-5}$/s for the $\epsilon = 1000$ mW/kg profile (see *Lübken* [1992] for more details). It is obvious from Figure 2 that the measured spectrum is not compatible even with very weak turbulence and that the fluctuations are much smaller than expected if turbulence were present. We note that the smallest ϵ value used in Figure 2 is close to the theoretical lower limit of turbulence, $\epsilon_{min} \sim \nu \cdot \omega_B^2$, which is on the order of 0.5–1 mW/kg at these altitudes. We conclude that there is no turbulence present in altitude bins with spectra similar to that shown in Figure 2, i.e., $\epsilon = 0$ mW/kg in these cases.

[10] In Table 2 we summarize the energy dissipation rates measured during the flights listed in Table 1. Minor changes have been made regarding the data analysis procedure compared to the compilation of ϵ values published by *Lübken* [1997]. We have reduced the altitude bin size from 5 km to 1 km to allow for a more detailed comparison with the radar observations of PMSE (the altitude resolution of the radars used in this study is typically 300 m). Furthermore, we have added the results from flight MDMI05 from July 1999. The individual ϵ profiles shown in Figure 3 are very structured with values ranging from $\epsilon = 0$ mW/kg up to $\epsilon \sim 2400$ mW/kg (the latter corresponds to a very large heating rate of ~200 K/d). A mean profile was calculated (taking into account the $\epsilon = 0$ mW/kg values) and smoothed by a 5 point running mean. As can be seen from Figure 3 this mean profile does not significantly deviate from the mean profile shown by *Lübken* [1997] which demonstrates that the changes in the data analysis procedure mentioned above have not significantly affected the mean profile (typical deviations between "old" and "new" mean values are less than appr. 20–30%). A detailed comparison of the individual turbulence profiles and PMSE is presented in section 3.

2.2. Polar Mesosphere Summer Echoes

[11] The rocket flights listed in Table 1 were accompanied by PMSE measurements from VHF radars, namely the Cornell University Portable Radar Interferometer (CUPRI) at 46.9 MHz in Esrange (flights NAT13, NBT05), the European Incoherent Scatter Radar (EISCAT) at 224 MHz in Tromsø (69°N; flights SCT03, SCT06) the ALOMAR-SOUSY radar (Arctic Lidar Observatory for Middle Atmosphere Research / Sounding System) at 53.5 MHz in Andøya (flights ECT02, ECT07, ECT12), and the ALOMAR wind radar (ALWIN) at 53.5 MHz in Andøya (flight MDMI05).

Table 2. Energy Dissipation Rates in mW/kg Deduced From the Ionization Gauge Measurements Listed in Table 1 as a Function of Altitude (z)

z, km	NAT13	NBT05	SCT03	SCT06	ECT02	ECT07	ECT12	MDMI05
80	0.0	0.0	0.0	0.0	0.0	0.0	0.0	0.0
81	0.0	0.0	0.0	0.0	0.0	0.0	0.0	0.0
82	0.0	3.2	0.0	0.0	0.0	0.0	0.0	0.0
83	0.0	5.6	0.0	0.0	0.0	0.0	0.0	6.3
84	0.0	0.0	0.0	0.0	0.0	0.0	1.6	0.0
85	0.0	0.0	2459.6	0.0	0.0	63.7	8.7	0.0
86	0.0	0.0	17.0	0.0	0.0	20.1	24.4	17.4
87	46.3	2.9	0.0	7.4	0.0	31.5	0.0	138.4
88	13.9	1182.7	142.9	351.1	116.2	35.2	119.7	87.4
89	0.0	1045.7	5.9	1538.2	37.8	0.0	0.0	0.0
90	0.0	70.5	0.0	95.7	105.3	0.0	59.4	0.0
91	0.0	109.9	0.0	108.9	0.0	0.0	5.6	0.0
92	255.5	14.0	0.0	131.5	0.0	0.0	0.0	0.0
93	65.6	0.0	0.0	0.0	111.9	0.0	0.0	0.0
94	364.7	0.0	0.0	0.0	0.0	0.0	0.0	0.0

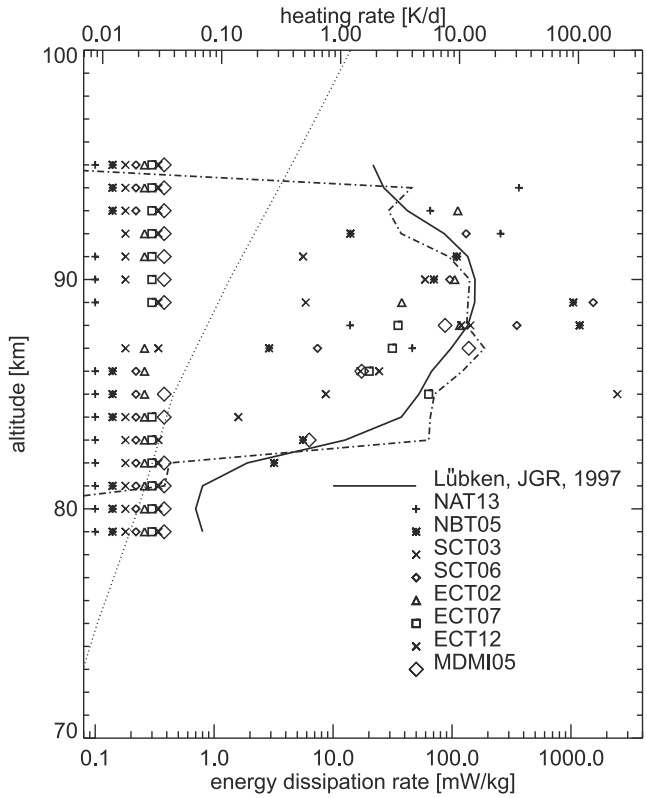

Figure 3. Turbulent energy dissipation rates ϵ for all flights listed in Table 1. Altitudes with no turbulence (i.e., $\epsilon = 0$ mW/kg) are indicated on the left ordinate. The mean profile (dotted-dashed line) was smoothed by a 5 point running mean. The dotted line indicates the theoretical lower limit given by $\epsilon_{min} \sim \nu \cdot \omega_B^2$ (ν = kinematic viscosity; ω_B = Brunt-Väisälä frequency). The mean profile from *Lübken* [1997] is shown for comparison (solid line). Energy dissipation rates are converted to heating rates (upper scale) using $dT/dt = \epsilon/c_p$ where c_p is the heat capacity of air at constant pressure.

Details of the radars are presented in the literature [*Swartz et al.*, 1993; *Bremer et al.*, 1996; *Latteck et al.*, 1999]. A typical horizontal distance between the location where the payloads pass through the 85 km height level and the radar beams at this altitude is 70 km. A comparison of PMSE measurements by the ALOMAR-SOUSY and the EISCAT radar (horizontal distance: ~120 km) was performed during the ECHO-94 campaign and showed general agreement in the temporal and height dependent structures observed by both radars [*Bremer et al.*, 1996]. This demonstrates that PMSE are fairly extended in their horizontal dimension and that it is appropriate to assume that the snap shot measurements taken during the rocket flights are representative for the PMSE situation during that flight in general. Since the radars used in this study are not absolutely calibrated it makes little sense to use the back-scattered power from different radars for a comparison with turbulence or with temperatures.

[12] The PMSE layers presented in this study are located between 82 and 89 km with a maximum occurrence and strength around ~85 km which is in general agreement with a statistical analysis of PMSE based on data from several years [*Hoffmann et al.*, 1999].

2.3. Temperatures

[13] Since the mid 1980s temperatures at high latitudes are deduced from in-situ measurements of densities by the "falling sphere" technique [*Schmidlin*, 1991; *Lübken*, 1999]. A small rocket transports a folded up sphere, made of metalized mylar, to an altitude of typically 110 km. After it is released the sphere inflates to 1-m diameter and passively falls through the atmosphere whereby it decelerates. A high-precision radar tracks the descent trajectory which is then used in the equations of motion to determine atmospheric density and horizontal winds. Temperatures are obtained by integrating the density profile assuming hydrostatic equilibrium. The height-dependent sphere reaction time-constant causes a smoothing of the density, temperature, and wind profiles. The smallest scales detectable are typically 8, 3, and 0.8 km at 85, 60, and 40 km, respectively. The uncertainty of the temperature data is typically 7, 3, and 1.5 K at 90, 80, and 70 km altitude, respectively [*Schmidlin*, 1991]. A summary of all measurements available at high latitudes during summer is presented by *Lübken* [1999].

[14] The ionization gauge measurements introduced in section 2.1 have also been used to derive absolute atmospheric number densities. The gauges were calibrated in a wind tunnel and Monte Carlo simulations were performed to allow for a correction of aerodynamical effects ("ram effect") encountered during flight [*Rapp et al.*, 2001]. Finally, high spatial resolution ($\Delta z \sim 100-200$ m) temperature profiles in the altitude range from 70 to 110 km with a typical accuracy of 2% were derived [*Rapp et al.*, 2002].

3. Comparison of Neutral Air Turbulence, Temperatures, and PMSE

3.1. Neutral Air Turbulence and PMSE

[15] A comparison of turbulence and PMSE for the 8 flights listed in Table 1 is shown in Figure 4. In most cases the PMSE show a single layered structure except in flights NBT05 and ECT02 where two layers are identified. In the latter cases neutral turbulence is restricted to the upper part of the PMSE layer with medium (ECT02) and very strong (NBT05) turbulence intensities. Some relatively strong turbulence is found above the double-layered PMSE.

[16] In the 6 flights with single layer PMSE there is only one case (SCT03) where very strong turbulence is found in the center of the layer and in only 2 cases (ECT12 and MDMI05) some weak turbulence is found at the lower edge or below the PMSE. It is obvious from the comparison shown in Figure 4 that there is no close correlation between PMSE and turbulence and that in fact turbulence is absent in most PMSE layers but is frequently observed above the PMSE. Counting the double layered PMSE from NBT05 and ECT02 as two separate events we arrive at a total of 10 layers. Strong or moderate turbulence is observed in only 3 out of these 10 cases. In all 8 flights turbulence is observed above the PMSE layer, sometimes very strong (SCT06).

[17] We have performed a statistical analysis for the 1 km altitude bins shown in Figure 4. An altitude bin is attributed

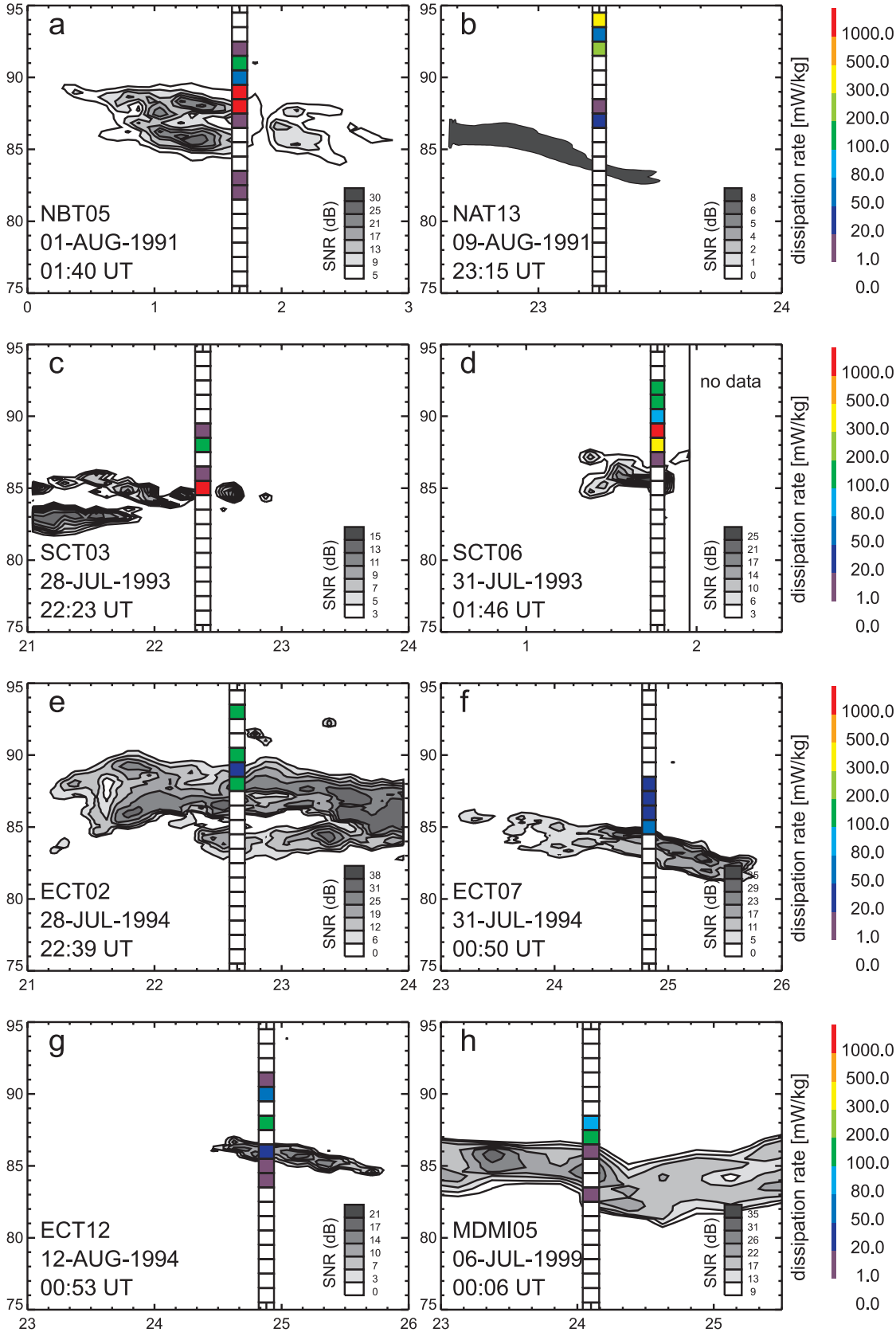

Figure 4. (a–h) Comparison of turbulent energy dissipation rates ϵ (color coded) and the PMSE intensity for the flights listed in Table 1. The PMSE data from flights NAT13 and NBT05 were taken from the literature [*Swartz et al.*, 1993; *Cho et al.*, 1993].

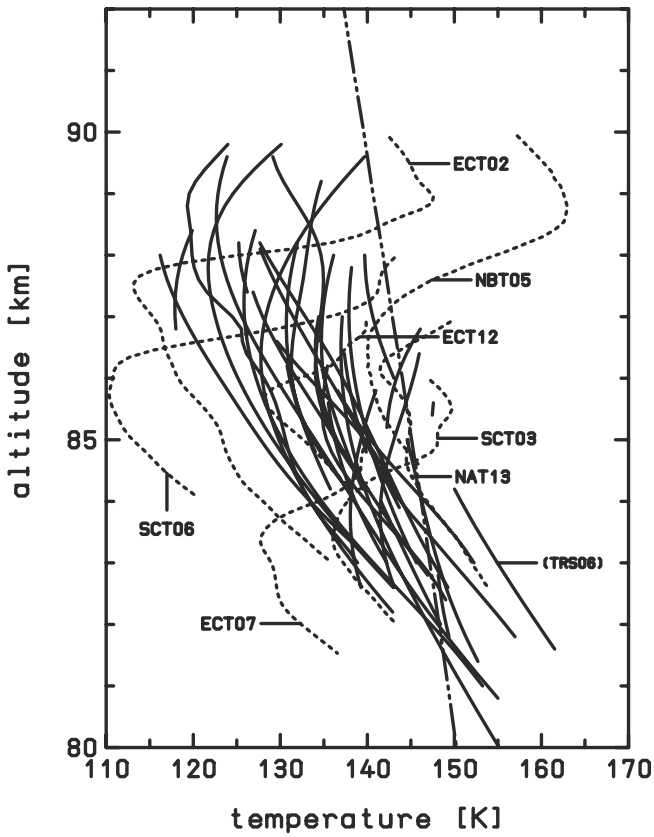

Figure 5. Temperature profiles measured within PMSE layers. Measurements by the falling sphere technique (solid lines) and by the TOTAL/CONE ionization gauges (dotted lines) are shown. The dotted-dashed line presents the frost point temperature profile using the model H_2O values from *Körner and Sonnemann* [2001].

to PMSE when a radar echo was present in a time slot of $\sim \pm 1/2$ hour around the rocket flight. We thereby take into account the uncertainty due to the horizontal distance between radar and in situ measurements. With this classification there are 31 altitude bins with PMSE out of which only 14 contain turbulence, i.e., at more than 50% of all PMSE altitudes there is no neutral air turbulence present. In cases where PMSE and turbulence coincide, the mean ϵ is 390 mW/kg with a rather large variability (standard deviation from the mean is 190 mW/kg). This mean value is mainly weighted by the rather large values observed in flights NBT05 and SCT03. The number of altitude bins with turbulence but no PMSE is 27 where in the majority of these cases (24 from 27) the turbulence layer is located above the PMSE. The mean ϵ value outside the PMSE layers is 132 mW/kg (not taking into account the layers with no turbulence, i.e., where $\epsilon = 0$ mW/kg). We have not made any attempt to correlate PMSE strengths to turbulence intensities since the absolute value of radar echo power depends on various unknown instrumental parameters (sensitivity etc.) which vary from one radar to the other.

[18] We conclude from the experimental data that there is no apparent correlation between PMSE and neutral air turbulence. In most cases PMSE exists without turbulence and strong turbulence is found above PMSE altitudes.

3.2. Neutral Air Temperature and PMSE

[19] We now come to a comparison of temperatures and PMSE. We have been fairly generous when defining the altitude range where PMSE exists during the rocket flight taking into account the uncertainty introduced by the spatial distance between the rocket and the radar measurements. We have therefore considered the echo power in a time slot of approximately $\pm 1/2$ h around the rocket launch. A summary of all temperatures measured by the falling sphere technique within a PMSE layer is shown in Figure 5. The corresponding profiles of the degree of saturation for water vapor over ice are shown in Figure 6 where we have used the model H_2O values from *Körner and Sonnemann* [2001]. As can be seen from these Figures the temperatures in the PMSE layers are generally below $\sim$150°K and the degree of saturation is generally larger than unity, i.e., it is generally cold enough at PMSE altitudes for water ice particles to exist or to grow. Even at temperatures larger than 150°K, say at 155°K, it takes tens of minutes for a 10 nm particle to evaporate assuming reasonable water vapor mixing ratios. In one FS profile (flight TRS06 on 23. August 1999 at 10:30 UT) the temperatures within the PMSE layer are

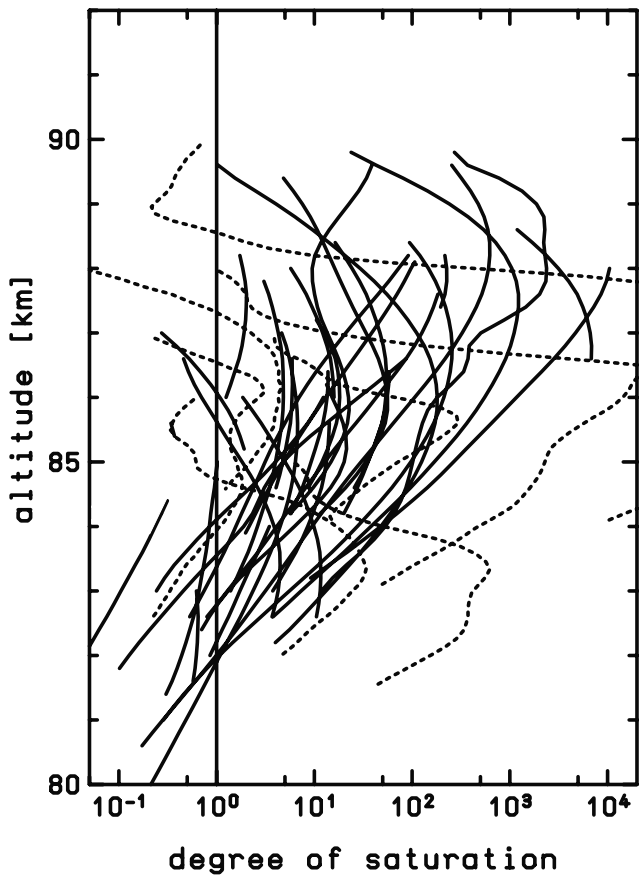

Figure 6. Degree of saturation of water vapor over ice (S) derived from the temperature profiles shown in Figure 5 using water vapor mixing ratios from *Körner and Sonnemann* [2001]. For S > 1 ice particles grow and for S < 1 they evaporate.

Table 3. Mean Temperature Lapse Rate Within the PMSE Layer ($\langle dT/dz \rangle$) and Its RMS Variability (RMS) for the Rocket Flights Listed in Table 1[a]

Flight Label	Altitude Range, km	$\langle dT/dz \rangle$, K/km	RMS, K/km
NAT13	82.5–87.0	−0.9	5.1
NBT05	84.5–90.0	1.9	7.7
SCT03	82.0–86.0	0.8	6.3
SCT06	84.0–88.0	5.8	13.1
ECT02	83.0–90.0	1.1	12.1
ECT07	81.5–85.0	1.0	6.7
ECT12	84.0–87.0	1.0	6.7

[a]No temperatures were derived for flight MDMI05 due to uncertain aerodynamic corrections caused by large coning of the payload.

rather large (up to 161 K at ~82 km) which corresponds to an evaporation time of a 1–3 minutes only. A closer inspection showed that indeed the PMSE had disappeared 10 minutes prior to the FS launch.

[20] In Figure 5 we also show high resolution temperature profiles within the PMSE layer derived from the TOTAL/CONE instruments. As mentioned above we have used a fairly generous definition of PMSE altitudes. For example, for flight NAT13 we have defined the PMSE altitude range as 82.5–87.0 since this is the range where PMSE where observed within a period of ~ ±1/2h around the rocket launch (see Figure 4b), whereas at the launch time the PMSE was actually restricted to a much narrower altitude range (~83.5–84.1). The altitude ranges of PMSE are listed in Table 3. It is obvious from Figure 5 that the high resolution TOTAL/CONE measurements basically confirm the results from the FS profiles, i.e., that at PMSE altitudes it is cold enough for water ice particles to exist. There is one exception, namely the upper part of flight NBT05 where temperatures exceed 160 K which corresponds to an evaporation time of only a few minutes for a 10 nm particle. Closer inspection of Figure 4a shows in fact that the PMSE had disappeared in the upper layer a few minutes prior to the CONE flight. This is a remarkable correlation between the appearance of PMSE and the thermal structure.

[21] In Figure 7 the high resolution temperature profiles measured by TOTAL/CONE are shown together with the PMSE layer measured some time around the sounding rocket flight. In all cases the PMSE is found at a local temperature minimum which is not necessarily the coldest place during that flight. It is interesting to note that the PMSE layer is confined to the local temperature minimum although it can be cold enough for ice particles to exist also at other altitudes. For example, in flight ECT07 the temperatures are below 150°K between approximately 80 and 91 km but the PMSE is confined to a relatively small altitude range from 82 to 85 km.

[22] In Figure 8 a high resolution temperature profile measured by CONE in flight ECT02 is shown together with the PMSE profile measured during that flight. It is interesting to note that the temperature lapse rate within the PMSE layer is not close to the adiabatic lapse rate as one would expect if persistent turbulent mixing has influenced the main background thermal structure. This result is confirmed by the other TOTAL/CONE flights as can be seen from Table 3 where we have listed the mean temperature lapse rates and their variability within the PMSE layer (for flight MDMI05 a temperature profile could not be obtained due to large coning of the payload which makes the ram correction mentioned in section 2.1 rather uncertain). Typical lapse rates within the PMSE layer are +1–2 K/km with a rather large variability of typically ±5–10 K/km. In none of the flights we have found an adiabatic lapse rate within the PMSE layers.

4. Discussion

[23] In the majority of the PMSE layers presented in this paper no neutral air turbulence is observed. This suggests that neutral air turbulence is not the prime cause of PMSE. We can even speculate that the occasional coincidence of neutral air turbulence and PMSE is accidental and that there is actually no common physical process behind these phenomena, except the background temperature profile which supports the creation of ice particles due to very low temperatures and which provokes the breaking of gravity waves and the production of turbulence due to the change in temperature gradient at the summer mesopause. This idea is further supported by the fact that the temperature gradient within the PMSE layer is not close to the adiabatic lapse rate which suggests that turbulence cannot have been active for a substantial time period since persistent turbulent mixing drives the background atmosphere towards the adiabatic lapse rate [*Hill et al.*, 1999]. A typical time constant required for this process is the time for turbulent transport which is on the order of 15–30 minutes considering typical turbulent velocities of 1–2 m/s and a layer thickness of 1–4 km. Therefore, if turbulence were present at PMSE altitudes for several hours we would expect to measure an adiabatic temperature lapse rate, contrary to the observations (see Table 3).

[24] Further support for the idea that the presence of turbulence at PMSE altitudes could be accidental rather than the cause for PMSE comes from the spectral broadening of the received radar signal which sometimes shows a dynamically quiet situation which suddenly turns to very disturbed conditions (see Figure 5 of *Cho and Röttger* [1997]). This suggests that PMSE is already present when turbulence sets in at the same altitudes. In this case the structures caused by an unidentified process cause PMSE and act as passive tracers for turbulence.

[25] We note, however, that some arguments are in favor of the creation of PMSE by turbulence, at least in some cases. Occasionally, excellent agreement has been found between the turbulence theory of PMSE and observations. The deduction of the Schmidt number (Sc) from the spectra of neutral air and electron number density fluctuations agrees nicely with the totally independent derivation of Sc based on simultaneous measurements of microphysical ice particle parameters [*Lübken et al.*, 1998]. It seems rather unlikely that this nice agreement is accidental and has no physical relationship to PMSE. We conclude that the question whether the occasional coincidence of some PMSE layers with turbulence is accidental or is due to a close physical connection remains open. This should not be confused with the fact that the majority of the PMSE layers are clearly not related to turbulence.

[26] Various theories are available in the literature which have tried to explain PMSE in terms of neutral air turbulence

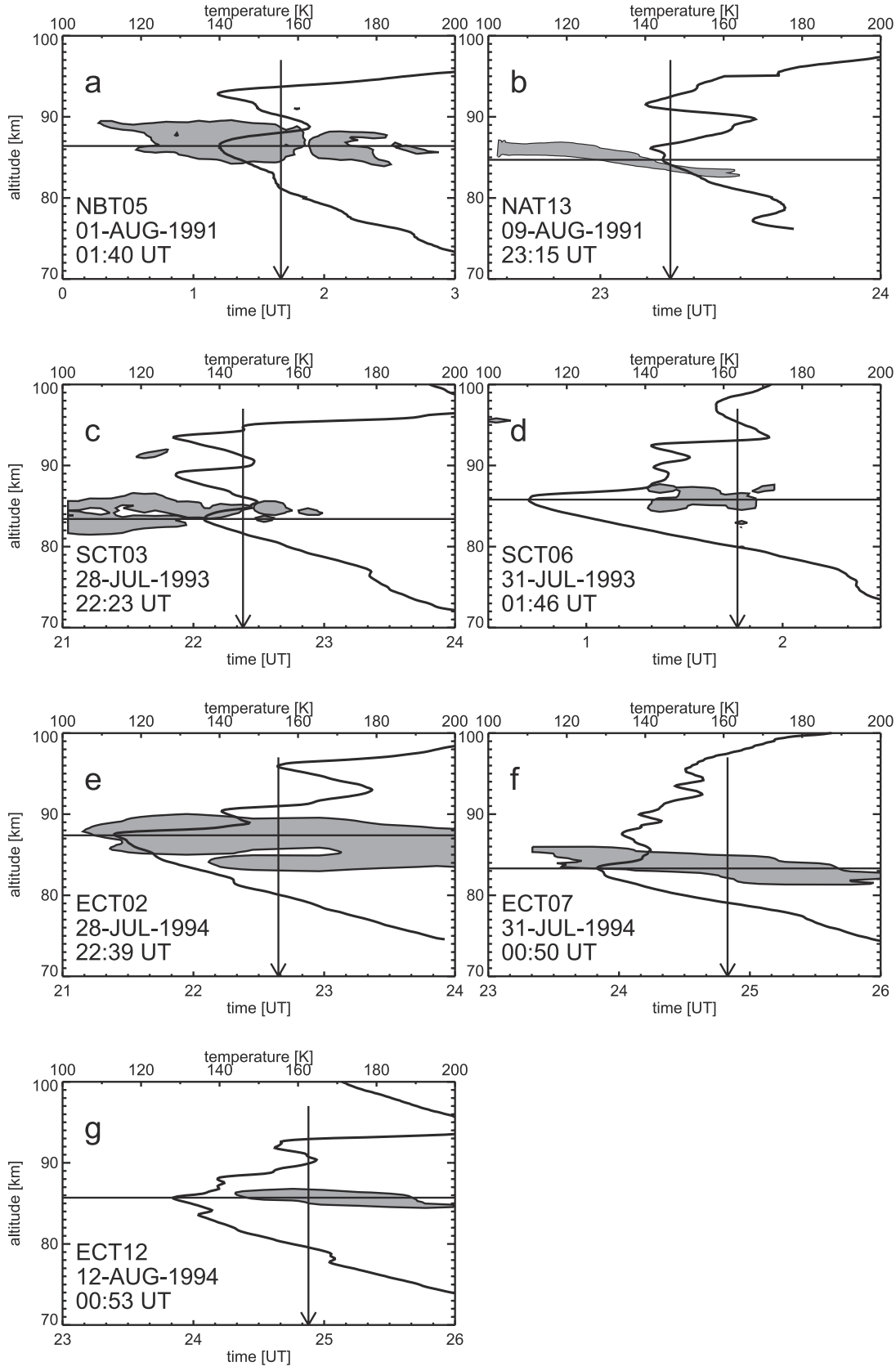

Figure 7. (a–g) Temperature profiles measured by TOTAL/CONE (solid lines, upper abscissa) compared with the PMSE measured some time around the rocket flight. A typical experimental temperature error is ±2–3 K [*Rapp et al.*, 2001]. The vertical line in each plot marks the rocket launch time. The horizontal line indicates the local temperature minimum close to the PMSE altitude.

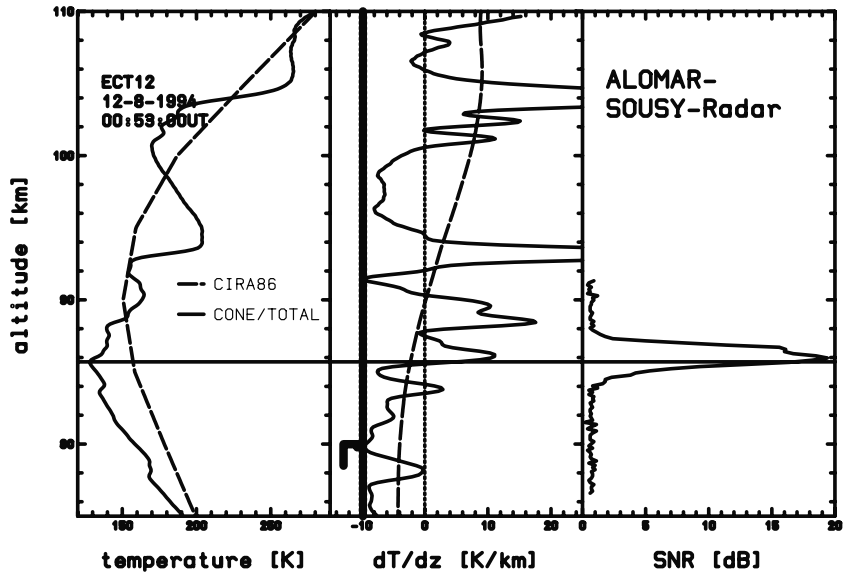

Figure 8. Temperature profile (solid line in left panel) derived from CONE measurements during flight ECT02 (see Table 1) and the PMSE profile measured during that flight (right panel). The CIRA-1986 profile is shown for comparison [*Fleming et al.*, 1990]. The temperature lapse rate (dT/dz) is shown in the middle panel. The adiabatic lapse rate ($-g/c_p$) and the isothermal case (dT/dt = 0 K/km) are shown for comparison (thick and thin dotted lines, respectively).

or by some other process involving neutral gas dynamics [*Kelley et al.*, 1990; *Havnes et al.*, 1992; *Cho and Röttger*, 1997; *Klostermeyer*, 1997; *Hill et al.*, 1999]. It is obvious from the data presented in the preceding sections that these theories are not applicable in the majority of PMSE events since we do not find significant neutral air density disturbances.

[27] It is interesting to note that even strong turbulence can be present around the mesopause but no PMSE is observed (see for example flight SCT06, Figure 4d). Obviously no significant electron density fluctuations at the radar Bragg scale are created presumably because the ice particles have not yet grown large enough to significantly reduce the diffusivity of the electrons. This explanation is in general agreement with standard ice particle growth and sedimentation theories [*Jensen and Thomas*, 1988] and supports the idea that aerosols must exceed a certain size and must be charged to reduce the electron diffusivity and to create PMSE [*Cho et al.*, 1992; *Rapp and Lübken*, 2000].

[28] Our temperature measurements show that within the PMSE layer it is always cold enough for ice particles to exist (except in two cases discussed above) which supports the general understanding that PMSE are closely related to water ice particles. This allows some insight in the thermal structure at places where radar observations have been made but where temperature measurements are not available [*Balsley et al.*, 1993; *Rüster et al.*, 2001].

[29] The high resolution TOTAL/CONE temperature profiles shown in Figure 7 demonstrate that the PMSE layers are basically centered around a local temperature minimum generated, e.g., by gravity waves. This is consistent with the findings of *Rapp et al.* [2002] who observed and modeled a close correlation between NLC and the local temperature minimum. It is further interesting to note that the PMSE layers cover only a part of the altitude range where the temperatures are low enough for ice particles to exist. This demonstrates that a low enough temperature is a necessary but not sufficient condition for PMSE to exist. We conclude that the nonappearance of PMSE in the upper summer mesosphere does not necessarily imply that temperatures are too high, since other ingredients are required to create strong radar echoes such as sufficient number of electrons, enough water vapor, and a structuring mechanism.

5. Conclusion

[30] Since the first observations of PMSE more than 20 years ago it was often taken for granted that these strong echoes must be caused by neutral air turbulence which affects the plasma. The measurements presented above suggest, however, that neutral turbulence plays a minor role in creating PMSE and that another, not yet identified mechanism must be at work instead. There is no doubt that small-scale fluctuations in the electron gas give rise to PMSE. However, the main physical process causing these fluctuations has not yet been identified. Any future theory of nonturbulent PMSE must consider the observational fact that in these cases neutral air is not affected at medium and small scales.

[31] All simultaneous measurements of temperatures and radar echoes show that at PMSE altitudes it is cold enough for ice particles to exist in agreement with the seasonal variation of PMSE and the thermal structure in the upper mesosphere. This again strengthens the close coupling between PMSE and the presence of ice particles. On the other hand, low enough temperatures are a necessary but not sufficient condition for PMSE to exist.

[32] It is important to understand the physical processes leading to PMSE since, in one way or the other, these strong echoes are related to geophysical relevant quantities, e.g.,

charged aerosols, very low temperatures, and plasma processes. From long term ground based radar measurements we can learn more about the temporal and spatial morphology of the background atmosphere and the microphysical processes leading to PMSE. We conclude from the data presented in this study that at least one of these processes, namely neutral air turbulence, plays a minor role in the creation mechanism of PMSE.

[33] **Acknowledgments.** The excellent work by the crew of the Mobile Raketenbasis (DLR, Germany) and the Andøya Rocket Range is gratefully acknowledged. We thank Ulf von Zahn and Jürgen Röttger for stimulating discussions. This project was supported by the Bundesministerium für Bildung, Wissenschaft, Forschung und Technologie, Bonn, under grants 01 OE 88027, 50 OE 9802 0, and 50 OE 99 01.

References

Balsley, B. B., R. F. Woodman, M. Sarango, J. Urbina, R. Rodriguez, E. Ragaini, and J. Carey, Southern-Hemisphere PMSE: Where are they?, *Geophys. Res. Lett.*, *20*, 1983–1985, 1993.

Bremer, J., P. Hoffmann, W. Singer, C. Meek, and R. Rüster, Simultaneous PMSE observations with ALOMAR-SOUSY and EISCAT-VHF radar during the ECHO-94 campaign, *Geophys. Res. Lett.*, *23*, 1075–1078, 1996.

Cho, J. Y. N., and J. Röttger, An updated review of polar mesosphere summer echoes: Observation, theory, and their relationship to noctilucent clouds and subvisible aerosols, *J. Geophys. Res.*, *102*, 2001–2020, 1997.

Cho, J. Y. N., T. M. Hall, and M. C. Kelley, On the role of charged aerosols in polar mesosphere summer echoes, *J. Geophys. Res.*, *97*, 875–886, 1992.

Cho, J., W. Swartz, M. Kelley, and C. Miller, CUPRI observations of PMSE during salvo B of NLC-91: Evidence of both partial reflection and turbulent scatter, *Geophys. Res. Lett.*, *20*, 2291–2294, 1993.

Czechowsky, P., R. Rüster, and G. Schmidt, Variations of mesospheric structures in different seasons, *Geophys. Res. Lett.*, *6*, 459–462, 1979.

Ecklund, W. L., and B. B. Balsley, Long-term observations of the arctic mesosphere with the MST radar at Poker Flat, Alaska, *J. Geophys. Res.*, *86*, 7775–7780, 1981.

Fleming, E. L., S. Chandra, J. J. Barnett, and M. Corney, Zonal mean temperature, pressure, zonal wind, and geopotential height as functions of latitude, *Adv. Space Res.*, *10*(12), 11–59, 1990.

Gadsden, M., and W. Schröder, *Noctilucent Clouds*, Springer-Verlag, New York, 1989.

Giebeler, J., F.-J. Lübken, and M. Nägele, CONE: A new sensor for in-situ observations of neutral and plasma density fluctuations, in *Proceedings of the 11th ESA Symposium on European Rocket and Balloon Programmes and Related Research, Montreux, Switzerland*, *Eur. Space Agency Spec. Publ., ESA-SP-355*, 311–318, 1993.

Havnes, O., F. Melandsø, C. L. Hoz, T. K. Aslaksen, and T. Hartquist, Charged dust in the Earth's mesopause: Effects on radar backscatter, *Phys. Scr.*, *45*, 535–544, 1992.

Havnes, O., J. Triøm, T. Blix, W. Mortensen, L. I. Næsheim, E. Thrane, and T. Tønnesen, First detection of charged dust particles in the Earth's mesosphere, *J. Geophys. Res.*, *101*, 10,839–10,847, 1996.

Hervig, M., R. Thompson, M. McHugh, L. Gordley, J. M. Russell III, and M. Summers, First confirmation that water ice is the primary component of polar mesospheric clouds, *Geophys. Res. Lett.*, *28*, 971–974, 2001.

Hill, R. J., D. E. Gibson-Wilde, J. A. Werne, and D. C. Fritts, Turbulence-induced fluctuations in ionization and application to PMSE, *Earth Planets Space*, *51*, 499–513, 1999.

Hillert, W., F.-J. Lübken, and G. Lehmacher, TOTAL: A rocket-borne instrument for high resolution measurements of neutral air turbulence during DYANA, *J. Atmos. Terr. Phys.*, *56*, 1835–1852, 1994.

Hoffmann, P., W. Singer, and J. Bremer, Mean seasonal and diurnal variations of PMSE and winds from 4 years of radar observations at ALOMAR, *Geophys. Res. Lett.*, *26*, 1525–1528, 1999.

Jensen, E., and G. E. Thomas, A growth-sedimentation model of polar mesospheric clouds: Comparions with SME measurements, *J. Geophys. Res.*, *93*, 2461–2473, 1988.

Kelley, M. C., D. T. Farley, and J. Röttger, The effect of cluster ions on anomalous VHF backscatter from the summer polar mesosphere, *Geophys. Res. Lett.*, *14*, 1031–1034, 1987.

Kelley, M. C., J. C. Ulwick, J. Röttger, B. Inhester, T. Hall, and T. Blix, Intense turbulence in the polar mesosphere: Rocket and radar measurements, *J. Atmos. Terr. Phys.*, *52*, 875–891, 1990.

Klostermeyer, J., A height- and time-dependent model of polar mesosphere summer echoes, *J. Geophys. Res.*, *102*, 6715–6727, 1997.

Körner, U., and G. R. Sonnemann, Global three-dimensional modeling of the water vapor concentration of the mesosphere-mesopause region and implications with respect to the noctilucent cloud region, *J. Geophys. Res.*, *106*, 9639–9651, 2001.

Latteck, R., W. Singer, and H. Bardey, The ALWIN MST radar: Technical design and performances, in *Proceedings of the 14th ESA Symposium on European Rocket and Balloon Programmes and Related Research, Potsdam, Germany*, *Eur. Space Agency Spec. Publ., (ESA SP-437), 179–184, 1999.*

Lübken, F.-J., On the extraction of turbulent parameters from atmospheric density fluctuations, *J. Geophys. Res.*, *97*, 20,385–20,395, 1992.

Lübken, F.-J., Seasonal variation of turbulent energy dissipation rates at high latitudes as determined by insitu measurements of neutral density fluctuations, *J. Geophys. Res.*, *102*, 13,441–13,456, 1997.

Lübken, F.-J., Thermal structure of the Arctic summer mesosphere, *J. Geophys. Res.*, *104*, 9135–9149, 1999.

Lübken, F.-J., G. Lehmacher, T. Blix, U.-P. Hoppe, E. Thrane, J. Cho, and W. Swartz, First in-situ observations of neutral and plasma density fluctuations within a PMSE layer, *Geophys. Res. Lett.*, *20*, 2311–2314, 1993.

Lübken, F.-J., J. Giebeler, T. Blix, E. Thrane, W. Singer, and J. Bremer, In situ measurement of the Schmidt number within a PMSE layer, *Geophys. Res. Lett.*, *21*, 1651–1654, 1994.

Lübken, F.-J., M. Rapp, T. Blix, and E. Thrane, Microphysical and turbulent measurements of the Schmidt number in the vicinity of polar mesosphere summer echoes, *Geophys. Res. Lett.*, *25*, 893–896, 1998.

Nussbaumer, V., K.-H. Fricke, M. Langer, W. Singer, and U. von Zahn, First simultaneous and common volume observations of noctilucent clouds and polar mesosphere summer echoes by lidar and radar, *J. Geophys. Res.*, *101*, 19,161–19,167, 1996.

Rapp, M., and F.-J. Lübken, Electron temperature control of PMSE, *Geophys. Res. Lett.*, *27*, 3285–3288, 2000.

Rapp, M., J. Gumbel, and F.-J. Lübken, Absolute density measurements in the middle atmosphere, *Ann. Geophys.*, *19*, 571–580, 2001.

Rapp, M., F.-J. Lübken, A. Müllemann, G. E. Thomas, and E. J. Jensen, Small-scale temperature variations in the vicinity of NLC: Experimental and model results, *J. Geophys. Res.*, *107*, 10.1029/2001JD001241, in press, 2002.

Rüster, R., J. Röttger, G. Schmidt, P. Czechowsky, and J. Klostermeyer, Observations of mesospheric summer echos at VHF in the polar cap region, *Geophys. Res. Lett.*, *28*, 1471–1474, 2001.

Schmidlin, F. J., The inflatable sphere: A technique for the accurate measurement of middle atmosphere temperatures, *J. Geophys. Res.*, *96*, 22,673–22,682, 1991.

Swartz, W., J. Cho, and C. Miller, CUPRI system configuration for NLC-91 and observations of PMSE during Salvo A, *Geophys. Res. Lett.*, *20*, 2287–2290, 1993.

Tatarskii, V. I., *The Effects of the Turbulent Atmosphere on Wave Propagation*, Isr. Program for Sci. Transl., Jerusalem, 1971.

Thrane, E. V., and B. Grandal, Observations of fine scale structure in the mesosphere and lower thermosphere, *J. Atmos. Terr. Phys.*, *43*, 179–189, 1981.

von Zahn, U., and J. Bremer, Simultaneous and common-volume observations of noctilucent clouds and polar mesosphere summer echoes, *Geophys. Res. Lett.*, *26*, 1521–1524, 1999.

P. Hoffmann, F.-J. Lübken, and M. Rapp, Leibniz-Institut für Atmosphärenphysik, Schloss-Strasse 6, 18225 Kühlungsborn, Germany. (luebken@iap-kborn.de)